Journal of ELECTRONIC MATERIALS, Vol. 38, No. 2, 2009
DOI: 10.1007/s11664-008-0545-x

An Investigation of Microstructure and Microhardness of Sn-Cu and Sn-Ag Solders as Functions of Alloy Composition and Cooling Rate

SUN-KYOUNG SEO,[1] SUNG K. KANG,[2] DA-YUAN SHIH,[2] and HYUCK MO LEE[1,3]

1.—Department of Materials Science and Engineering, KAIST, 335 Gwahangno, Yuseong-gu, Daejeon 305-701, Republic of Korea. 2.—IBM T.J. Watson Research Center, Yorktown Heights, NY 10598, USA. 3.—e-mail: hmlee@kaist.ac.kr

The microstructure and microhardness of Sn-*x*Ag and Sn-*x*Cu solders were investigated as functions of alloy composition and cooling rate. The Ag compositions examined varied from 0.5 wt.% to 3.5 wt.%, while Cu varied from 0.5 wt.% to 2.0 wt.%. Three cooling rates were employed during solidification: 0.02°C/s (furnace cooling), about 10°C/s (air cooling), and 100°C/s or higher (rapid solidification). Sn grain size and orientation were observed by cross-polarization light microscopy and electron-backscattering diffraction (EBSD) techniques. The microhardness was measured to correlate the mechanical properties with alloy compositions and cooling rates. From this study, it was found that both alloy composition and cooling rate can significantly affect the Sn grain size and hardness in Sn-rich solders. The critical factors that affect the microstructure–property relationships of Sn-rich solders are discussed, including grain size, crystal orientation, dendrite cells, twin boundaries, and intermetallic compounds (IMC).

Key words: Sn-Ag, Sn-Cu, microstructure, Sn grain, microhardness, cooling rate

INTRODUCTION

Sn-based, near-eutectic binary or ternary solder alloys are promising Pb-free candidates to replace Pb-containing solders in microelectronic packaging applications. The leading candidates include Sn-0.7Cu, Sn-3.5Ag, and Sn-3.8Ag-0.7Cu (all in wt.% unless specified otherwise). From the extensive research on Pb-free solders, the near-eutectic ternary Sn-Ag-Cu (SAC) solder alloys are recognized as the most promising candidate for surface-mounting (SMT) card assembly such as ball grid array (BGA) solder joints.[1–4] However, the near-eutectic Sn-Ag-Cu solder composition has not been accepted for C4 flip-chip interconnect application due to its high modulus and high yield strength. Another challenge with the near-eutectic Sn-Ag-Cu composition is the difficulty of producing solder bumps at fine pitch by a conventional wafer bumping method such as electroplating, although it is possible by the new emerging technologies such as C4NP[5] or ball placement.[6] For coarse-pitch applications, the solder paste screening technique is popularly used for bumping both wafer and substrate.

To mitigate the concerns of the near-eutectic ternary Sn-Ag-Cu solders, Sn-Ag or Sn-Cu binary systems, especially with a low Ag and/or Cu content, have been investigated to produce low modulus and more ductile solder joints.[7,8] However, reducing the alloying content in the binary and ternary Sn-based solders would significantly affect their microstructure and properties.

Since most Sn-rich solders contain more than 95 wt.% Sn, various physical, chemical, and

(Received April 11, 2008; accepted August 14, 2008; published online September 10, 2008)

mechanical properties of Sn-rich solders are predominantly affected by the properties of pure Sn. Different from Pb, which has an isotropic crystal of the face-centered cubic structure, Sn has a highly anisotropic crystal structure of body-centered tetragonal (bct). In the reported research, the same anisotropic properties as pure Sn were observed in the near-eutectic Sn-Ag-Cu solder, which affect the mechanical property of solder joints.[9,10]

Lehman et al.[11] reported that a few large Sn grains in BGA-size solder joints were observed in pure Sn, while the cyclic twinning structure was observed in near-eutectic ternary Sn-Ag-Cu and fine twinning structures were observed in near-eutectic binary Sn-Ag solders. However, it is not well understood how the alloying elements Ag and Cu affect the Sn grain structure and its associated mechanical properties.

In this study, the microstructure of low-Ag- or low-Cu-content solders is systematically investigated in terms of alloy composition and cooling rate. In addition, the effects of other minor alloying elements such as Ni or Zn are also investigated. To correlate the microstructure and grain orientation with the mechanical properties of Sn-rich solders, the microhardness of the corresponding solders is also evaluated in terms of alloy content and cooling rate.

EXPERIMENTAL

Sn-*x*Ag (*x*: 0 wt.%, 0.5 wt.%, 1.0 wt.%, and 1.8 wt.%; 380 μm diameter), Sn-3.5Ag (720 μm), Sn-*x*Cu (*x*: 0.5 wt.%, 1.0 wt.%, 1.5 wt.%, and 2.0 wt.%; 380 μm), Sn-1.8Ag-0.15Ni (380 μm), and Sn-3.8Ag-0.7Cu-0.7Zn (850 μm) solder balls, commercially produced, were used in this study. The Sn-0.5Ag-1.0Cu solder ball (480 μm) was produced in our laboratory. As-received solder balls were rapidly quenched at a rate of ≥100°C/s during their production by the supplier. The as-received solder balls were first reflowed at 250°C for 10 min in a vacuum oven and then cooled either in air (~10°C/s) or in furnace (~0.02°C/s). Because the melting temperature of the solder alloys is about 230°C, all solders were melted at 250°C.

The solder balls were cross-sectioned, fine-polished, and examined with an optical microscope under both bright-field and cross-polarized imaging conditions. Cross-polarized images revealed Sn grain structures, while bright-field images exhibited the β-Sn dendrites, intermetallic compound (IMC) particles, and their network structure. Different polishing techniques were employed for different imaging conditions. A well-polished, flat surface is required for cross-polarization images and EBSD study, while a slightly etched surface is used for bright-field images to detect the IMC phases. The optical cross-polarization imaging technique has been demonstrated to be a useful tool to evaluate the Sn grain size and to correlate with the results from EBSD work on grain orientation.[12] For the analysis of fine microstructures, the back-scattered (BS) electron mode of scanning electron microscopy (SEM) was used. Compositional analyses of the phases were also conducted with energy-dispersive x-ray spectroscopy (EDS) in an SEM.

For the thermodynamic calculations (binary phase diagrams and solubility calculations), the Thermo-Calc software developed at the Royal Institute of Technology, Stockholm, Sweden was used.[13] The reported binary parameters of Sn-Ag, Sn-Cu, and Sn-Ni were used in this study[14–16]; and the microhardness tests were performed using a 5 g force and a 5 s dwell time on the cross-sectioned surface of the solder balls. The Vickers hardness number (VHN) was reported as an average value by measuring 15 indentations or more.

RESULTS AND DISCUSSION

Microstructure of Sn-Ag solders

Figure 1 shows a collection of cross-polarized images of Sn-Ag solders as a function of Ag composition and cooling rate. Pure Sn exhibits one to three large grains in 380-μm-diameter balls, independent of cooling rate. However, when Ag is added, a fine-grained microstructure is observed. The grain structure becomes very fine, especially with fast cooling. In the rapidly quenched, as-received Sn-0.5Ag solder balls, about 50% of the balls have one to three large grains like pure Sn, and the remaining 50% have the fine structure as shown in Fig. 2. As the Ag content increases, the microstructure becomes finer and the ratio of the samples having the fine structure increases. For the quenched Sn-1.8Ag, over 90% have the fine structure. The similar fine structure of Sn-Ag was already reported by Lehman et al.[11] and Telang et al.[17] for an Ag content of 1.65 wt.% to 3.0 wt.% (near eutectic).

In slow cooling (air and furnace cooling), relatively large grains are observed in Sn-Ag solders, although some fine structure is still observed. Almost all samples have large grains. However, compared with pure Sn, the grain size is somewhat smaller in the case of low-Ag solders.

Figure 2 shows cross-polarized images of high-Ag, eutectic Sn-3.5Ag balls (720 μm) solidified at three different cooling rates. These microstructures show a mixture of large and fine grains regardless of the cooling rate. Comparing Figs. 1 (low Ag) and 2 (near-eutectic Ag), it is evident that the microstructure of low-Ag solders is sensitive to the cooling rate and Ag composition, but that of the high-Ag eutectic solder is not. The variations in microstructure appear to be independent of ball size.

The EBSD technique was employed to identify the crystal orientation of the fine structure of the Sn-Ag solder. Figure 3 shows an EBSD image taken from an area of 70 μm × 140 μm from the cross-sectioned surface of a rapidly quenched Sn-0.5Ag sample. Comparing the images in Fig. 3a (optical) and 3b (EBSD) it is noted that β-Sn cell boundaries do not

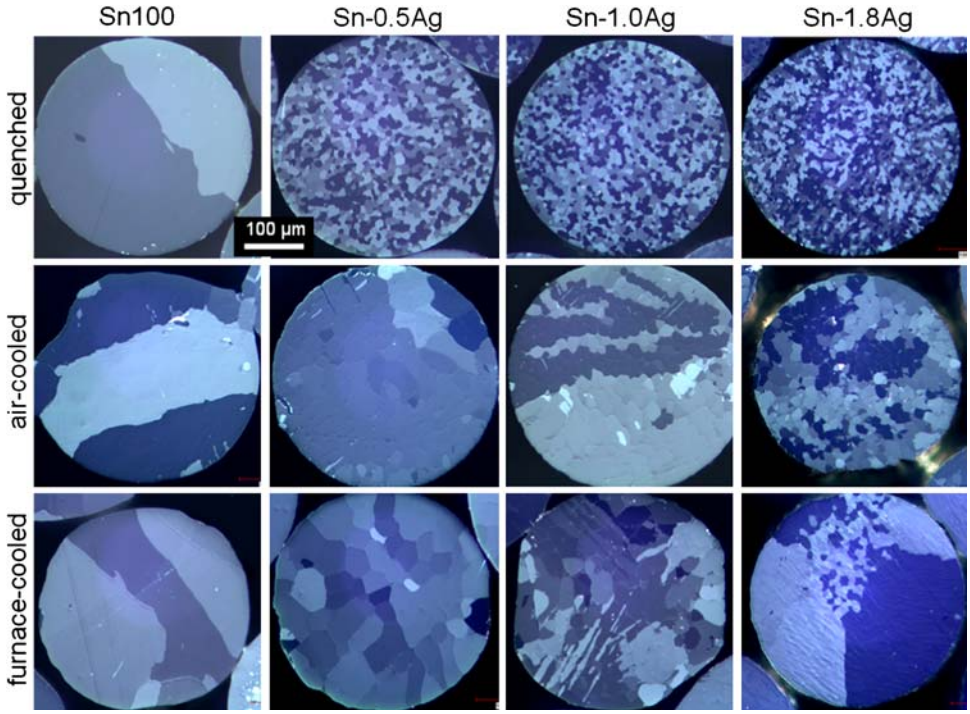

Fig. 1. Cross-polarized images of Sn-Ag solder balls (380 μm diameter) as a function of cooling rate and Ag composition (0 wt.%, 0.5 wt.%, 1.0 wt.%, and 1.8 wt.%).

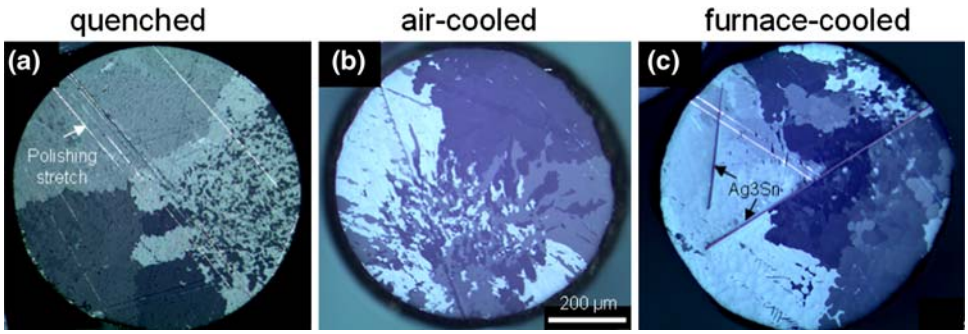

Fig. 2. Cross-polarized images of Sn-3.5Ag solder balls (720 μm diameter): (a) quenched, (b) air cooled, and (c) furnace cooled.

always match the grain boundaries. Several Sn dendrite cells can have the same crystal orientation to form one grain structure, showing as one color contrast in both the cross-polarized and EBSD images. From Fig. 3b, it is surprising to find that all grains have only three colors. From Fig. 3c, the crystal orientations are concentrated to three different points on the pole figure and inverse pole figure from the whole scanned area. In other words, there are only three crystal orientations in the fine-grain-appearing scanned area. The misorientation between two similar colors is smaller than 10 deg, and the misorientation between two different colors is about 60 deg. Therefore, as shown in Fig. 3d, the misorientation data are concentrated on low angles below 10 deg and near 60 deg. This is in good agreement with the report by Telang et al.,[17] for Sn-1.63Ag cooled at ~0.3°C/s.

The EBSD image of the fine-grained Sn-Ag solder reveals the cyclic twin structure with each grain rotated around the [100] axis of the Sn crystal by about 60 deg, and with the [100] axes of all the Sn crystals aligned in just one direction. The cyclic twinning of Sn-Ag-Cu solder was reported to consist of six twin regions turning on the [100] axis about 60 deg in one whole BGA solder ball. The faced regions of the same crystal direction were called a "beach-ball structure."[9,11] However, the cyclic twinning structure of Sn-Ag solders observed in this study is very fine (below 20 μm in average size) and repetitive across the entire area of a solder ball.

As shown in the Sn-rich side of the Sn-Ag binary phase diagram (Fig. 4) the eutectic composition of Sn-Ag is about 3.7 wt.% Ag, and three Ag contents examined in this study are depicted as the vertical

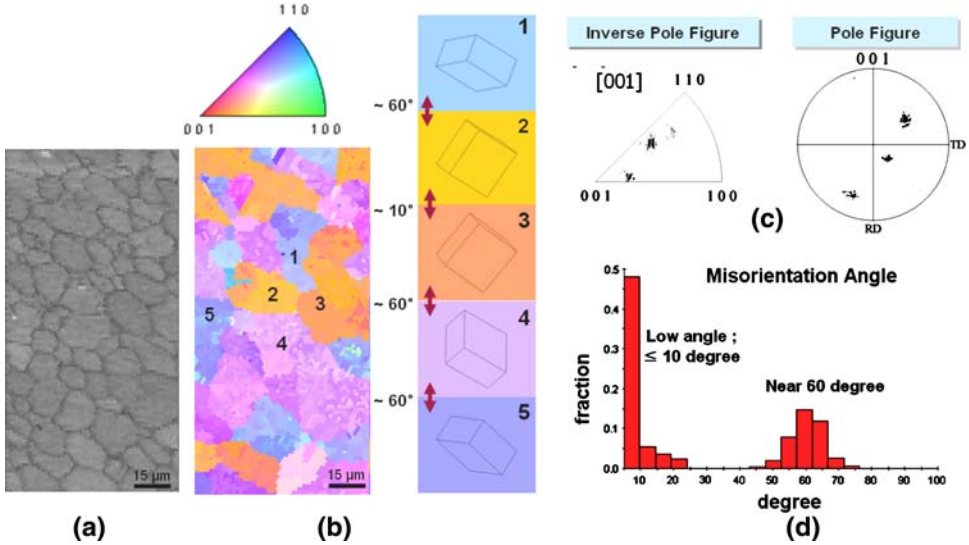

Fig. 3. EBSD data of Sn-0.5Ag quenched: (a) optical image, (b) EBSD image, (c) pole figure and inverse pole figure, and (d) misorientation graph.

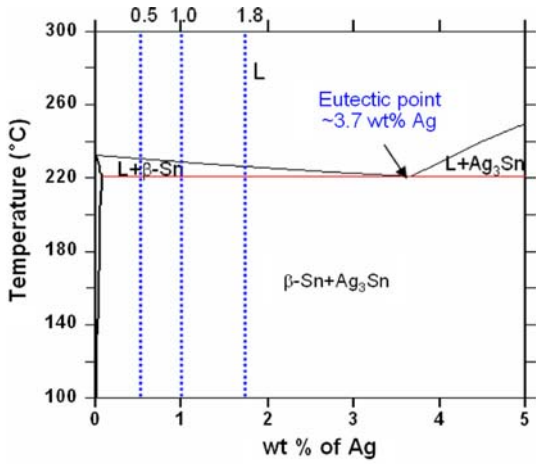

Fig. 4. The Sn-rich region of the calculated binary Sn-Ag phase diagram.

lines: 0.5Ag, 1.0Ag, and 1.8Ag. During cooling after the reflow at 250°C, the β-Sn phase would form first from the liquid, and then the Ag_3Sn phase precipitates along Sn dendrite cell boundaries. In our experiment, the microstructure of Sn-Ag solders was found to be highly sensitive to the cooling rate. As shown in Fig. 5, Sn dendrite boundaries are continuously decorated with an Ag-rich phase or Ag_3Sn particles with slow cooling (air cooled and furnace cooled), but the precipitation of an Ag-rich phase along the cell boundaries is not continuous in the rapidly cooled sample. This suggests that much more Ag solutes than predicted by the equilibrium phase diagram are supersaturated in the fast-cooled Sn matrix.

Table I shows the solubility of Cu, Ni, and Ag in Sn thermodynamically calculated using the literature information.[14–16] Ag has the largest solubility in Sn among the three elements. At a reflow temperature of 250°C, Ag has a solubility of 5.03 wt.% in the molten Sn. When slowly solidified, Ag atoms would exist as Ag_3Sn and solute atoms in the Sn matrix. For fast cooling, more Ag solute atoms can be frozen in the Sn matrix. This would facilitate the formation of the fine cyclic twins observed in Sn-Ag solders.

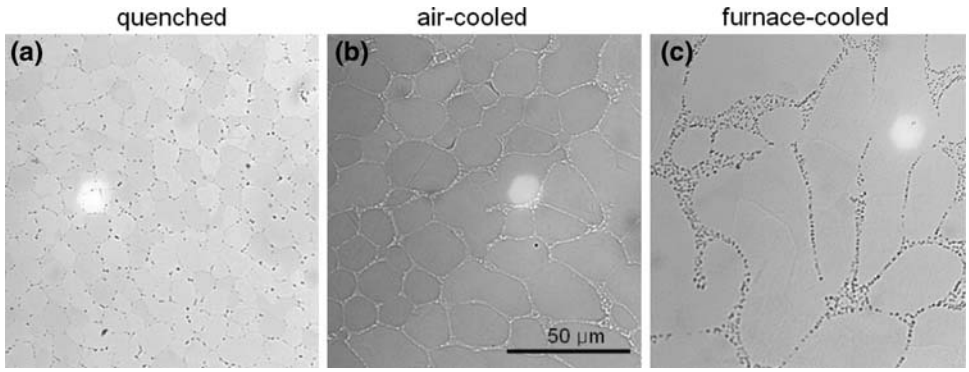

Fig. 5. Optical images of Sn-1.0Ag: (a) quenched, (b) air-cooled, and (c) furnace-cooled.

Table I. Solubility of Ag, Cu, and Ni in Sn

Temperature (°C), Phase	Solubility in Sn (wt.%)		
	Cu	Ni	Ag
300, Liquid	2.28	0.30	8.30
250, Liquid	1.23	0.198	5.03
200, β-Sn	0.00347	0.000935	0.052
50, β-Sn	0.0000379	0.00000352	0.002

Microstructure of Sn-Cu Solders

To compare the alloying effects of Ag versus Cu in Sn-rich solders, the microstructure of Sn-Cu solders was also investigated by changing the Cu content from 0.5 wt.% to 2.0 wt.%. Figure 6 shows a collection of cross-polarized images of Sn-Cu solders in terms of Cu composition and cooling rate. Low-Cu (0.5 wt.% and 1.0 wt.%) solders have one or two large Sn grains independent of the cooling rate. This situation is similar to the case of pure Sn, as shown in Fig. 1. However, the Sn grain structure of high-Cu (1.5 wt.% and 2.0 wt.%) solder is sensitive to the cooling rate. Large Sn grains are observed in the quenched samples, small grains (below 20 μm in average size) in the air-cooled, and a mixture of large and small grains in the furnace-cooled samples.

An EBSD experiment was conducted with the Sn-2.0Cu air-cooled sample with relatively small grains to obtain information about grain orientation. Since large Cu_6Sn_5 IMC particles raise the noise level in EBSD data, a smaller area ($\sim$60 μm $\times$ 60 μm) is scanned to avoid large IMCs. Figure 7 shows the EBSD result from two solder balls. Comparing the EBSD color contrasts and the point distribution in the pole and inverse-pole figures, a variety of crystal orientations are noted. The misorientations between neighboring grains are distributed over a wide range of 0 deg to 95 deg, as shown in Fig. 7d. From the misorientation data and Sn crystal images of each grain, the fine microstructure of the Sn-2.0Cu (air cooled) is regarded as the general grain structure, not the twinning structure as observed in Sn-Ag (Fig. 3).

In contrast to the fine twin structure observed in quenched Sn-Ag solders, the rapidly quenched Sn-Cu solders have large Sn grains regardless of the Cu content, as shown in Fig. 6. For the air-cooled and furnace-cooled samples, there is a trend for grain size reduction when the Cu content increases. In addition, the grains of the furnace-cooled samples are expected to become even coarser, resulting in somewhat larger grains than in the air-cooled samples. To compare the microstructural changes due to cooling rate, the microstructure of Sn-2.0Cu was examined by SEM and optical microscopy, as shown in Fig. 8. For rapid cooling (Fig. 8a), very fine Cu_6Sn_5 precipitates were uniformly distributed in the whole area. This yielded a large Sn grain structure after rapid cooling. In the air-cooled and furnace-cooled samples of Sn-2.0Cu (Fig. 8b and c), the large primary Cu_6Sn_5 phase is observed, as expected from the Sn-Cu binary phase diagram

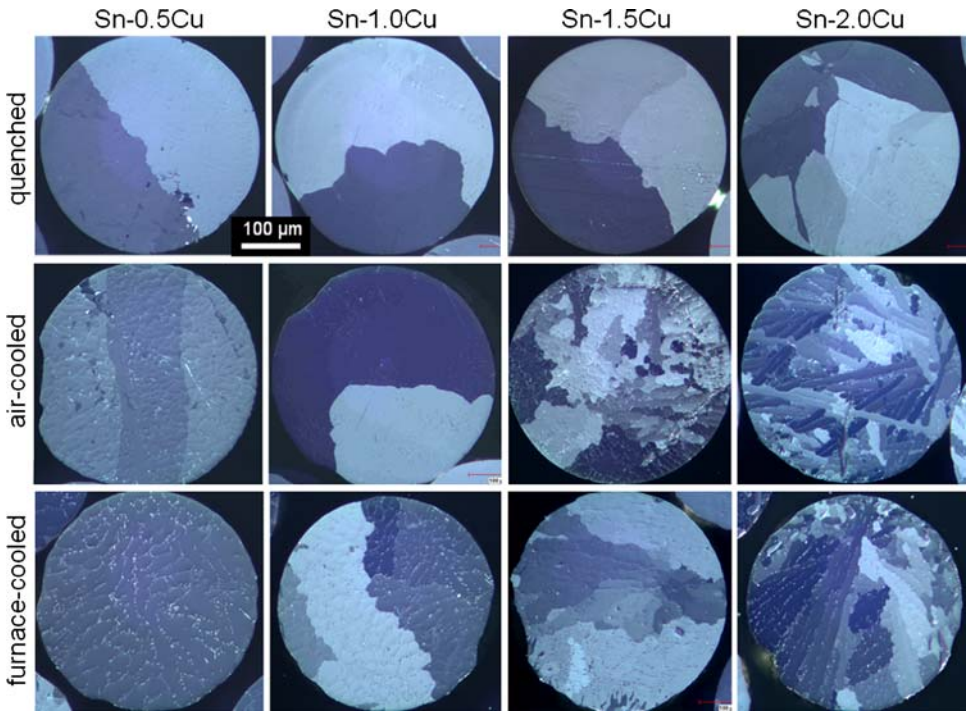

Fig. 6. Cross-polarized images of Sn-Cu solder balls (380 μm diameter) as a function of cooling rate and Cu composition (0.5 wt.%, 1.0 wt.%, 1.5 wt.%, and 2.0 wt.%).

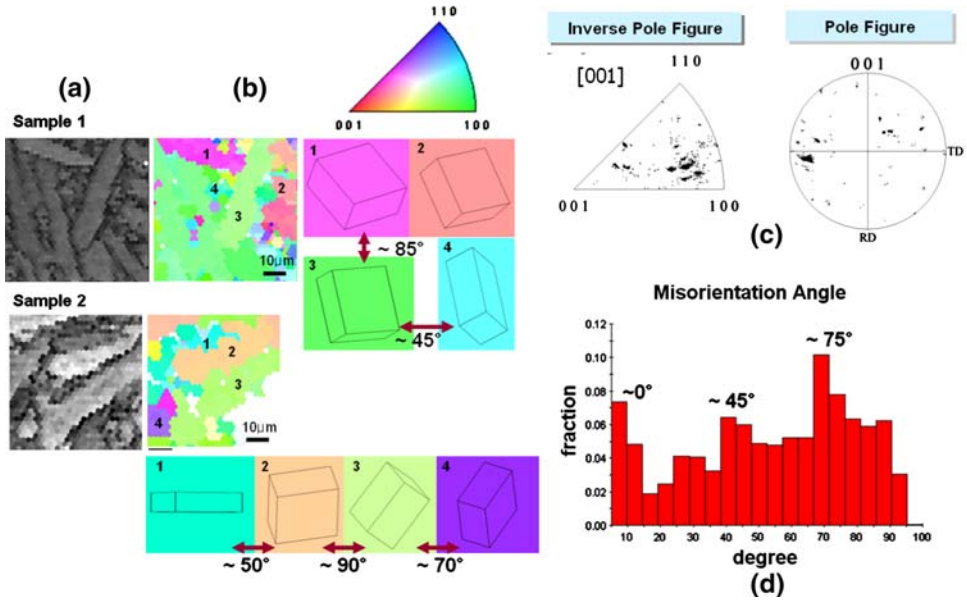

Fig. 7. EBSD data of Sn-2.0Cu, air-cooled: (a) optical image, (b) EBSD image, (c) pole figure and inverse pole figure, and (d) misorientation graph.

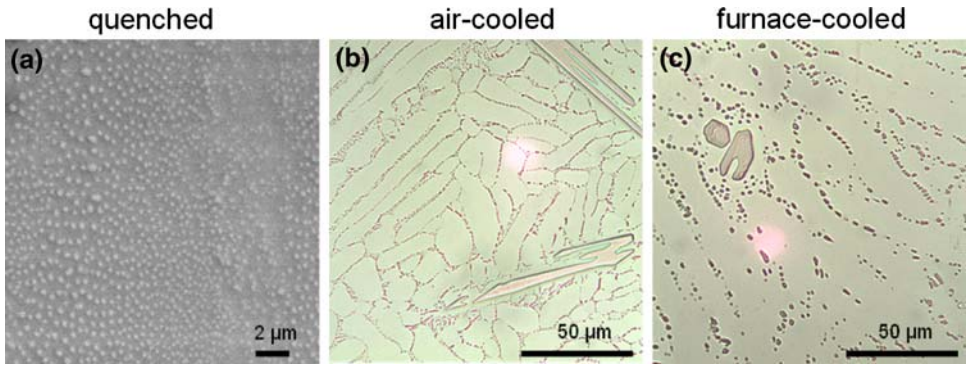

Fig. 8. SEM and optical images of Sn-2.0Cu (a) quenched, (b) air-cooled, and (c) furnace-cooled.

(Fig. 9). The large Cu_6Sn_5 phase that formed prior to β-Sn solidification could provide the additional nucleation sites for β-Sn dendrite cells. This could lead to various Sn crystal orientations, producing small Sn grains. In the furnace-cooled sample (Fig. 8c), β-Sn and IMC particles were further coarsened during solidification. Therefore, the Sn grain size with furnace cooling is somewhat larger than with air cooling.

The composition of the Sn-Ag-Cu solder having a "beach-ball" twinning structure was reported previously to be near eutectic.[9,11] In our investigation, the "beach-ball" twinning structure was also observed in a low-Ag Sn-0.5Ag-1.0Cu solder, as shown in Fig. 10. This phenomenon could be understood by combining the effects of Ag and Cu alloying additions to pure Sn as discussed earlier. In the study of the Sn-Ag system, it is shown that Ag addition to Sn promotes the formation of fine cyclic twinning. In the Sn-Cu system, it is also

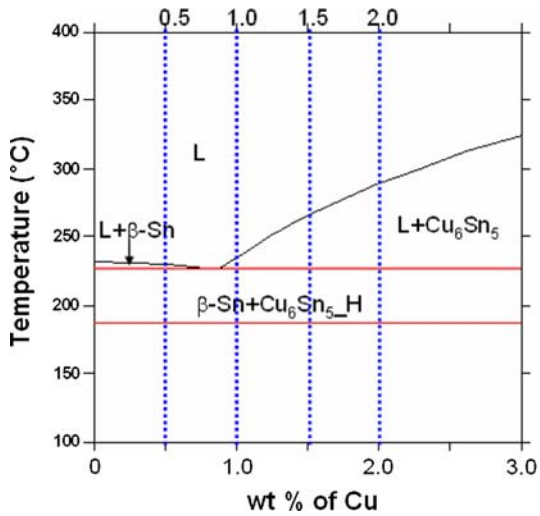

Fig. 9. The Sn-rich region of the calculated binary Sn-Cu phase diagram.

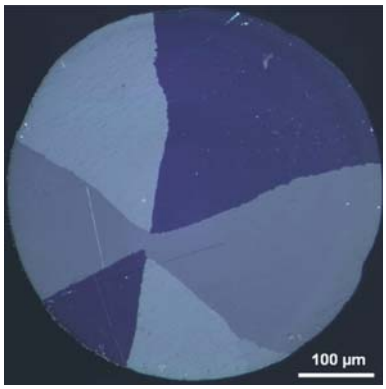

Fig. 10. Cross-polarized image of Sn-0.5Ag-1.0Cu, air-cooled (480 μm diameter).

demonstrated that Cu addition has a propensity to form large grains. These two trends combined could lead to a large cyclic "beach-ball" twinning like that shown in Fig. 10.

Effects of Minor Alloying Elements

Similar to Cu or Ag, a minor addition of Ni or Zn is shown to significantly affect the microstructure of Sn-rich solders. When 0.15 wt.% of Ni is added to Sn-Ag, the Sn grains become larger, as shown in Fig. 11a, as compared with the fine grain structure, shown in Fig. 1, of air-cooled Sn-1.8Ag. Similarly, when 0.7 wt.% of Zn is added to Sn-Ag-Cu, Sn grains become larger, as shown in Fig. 11b. These results could be explained by the undercooling effect of minor alloying elements during Sn solidification. If Ni or Zn is added to solder, the undercooling becomes smaller and consequently the microstructure (both Sn dendrite cells and eutectic structure) becomes coarser.[18–20] More specific results about the effects of minor elements on microstructure will be discussed in future publications.

Microhardness of Sn-Ag and Sn-Cu Solders

Microhardness tests were conducted to find the relationship between the microstructure and mechanical properties of the low-Ag and low-Cu, Sn-rich solders. Figure 12 shows the microhardness data of (a) Sn-Ag and (b) Sn-Cu solders as functions of alloy composition and cooling rate. Sn-Cu solders follow a general structure–property relationship, with higher hardness for greater alloying additions and faster cooling. However, Sn-Ag solders do not

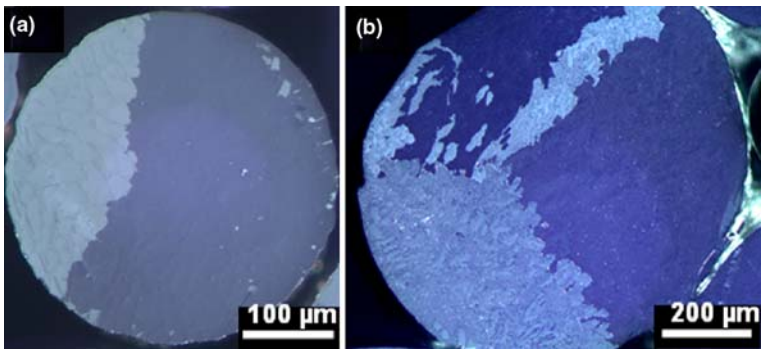

Fig. 11. Cross-polarized images of (a) Sn-1.8Ag-0.15Ni (380 μm diameter) and (b) Sn-3.8Ag-0.7Cu-0.7Zn (850 μm diameter), air cooled.

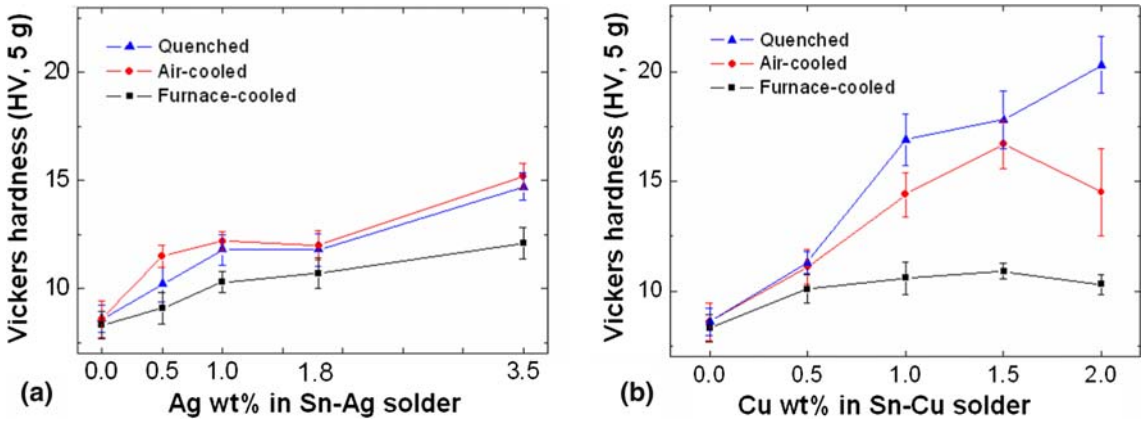

Fig. 12. Microhardness data of (a) Sn-Ag and (b) Sn-Cu solders.

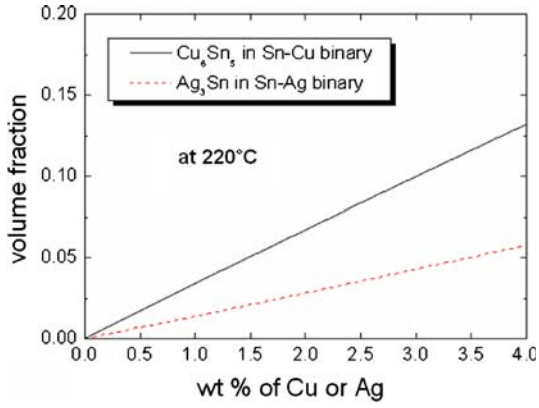

Fig. 13. The volume fraction of Cu_6Sn_5 and Ag_3Sn phases (to be formed at 220°C) as a function of Cu or Ag content in each binary system.

follow this relation in terms of cooling rate; the air-cooled samples were harder than the rapidly quenched samples, as shown in Fig. 12a. Sn-Ag quenched samples have the fine twin structure and Sn-Ag air-cooled samples have a relatively coarse microstructure, as revealed by the cross-polarized images in Fig. 1. Generally, the metals and alloys having a finer grain structure possess a higher yield strength and/or higher hardness owing to the grain boundary strengthening mechanism (known as the Hall-Petch relationship). However, the fine twin structure observed in Sn-Ag solders does not seem to contribute to the hardening of Sn-rich solders.

In search for a better correlation of the microhardness data with the microstructure, the distribution of IMC particles in Sn-1.0Ag was examined in bright-field images, as shown in Fig. 5. Due to the rapid solidification, the Ag-rich phase is not fully segregated along Sn dendrite cell boundaries in the quenched sample (Fig. 5a), while in the air-cooled sample the Ag_3Sn phase is continuously precipitated along the Sn cell boundaries, forming a continuous network of eutectic region (Fig. 5b). The continuous IMC network in the air-cooled Sn-1.0Ag sample is attributed to its higher hardness value than the rapidly quenched one. In the furnace-cooled sample (Fig. 5c) coarsening of the Ag_3Sn phase as well as Sn dendrite cells are responsible for the lower hardness values for the range of Ag content examined. From this observation, it is concluded that the microhardness values are better correlated with the characteristics and distribution of IMC particles (quantity, size) rather than with the Sn grain or twin size revealed in cross-polarizing images. Similar correlations between the hardness value and IMC characteristics are also exhibited by Sn-Cu solders.

The hardness of Sn-Ag or Sn-Cu solders generally increases as the content of Ag or Cu increases, as shown in Fig. 12. However, the hardness of Sn-Cu air-cooled solders increases until 0.15 wt.% Cu, after which a hardness drop is noted for Sn-2.0Cu. This hardness drop could be explained by confirming the presence of the large primary Cu_6Sn_5 in the Sn-2.0Cu air-cooled sample, as shown in Fig. 8b. In the furnace-cooled Sn-Cu solders, since most of the Cu atoms are precipitated as large phases of Cu_6Sn_5, the microhardness does not significantly increase as the Cu content increases.

Comparing the trends for increasing hardness in Sn-Ag and Sn-Cu, it is evident (by comparing the same amount of Ag or Cu addition at the same cooling rate) that the addition of Cu to Sn has a greater effect on hardness than does the addition of Ag. This can be due to two reasons. First, the volume fraction of Cu_6Sn_5, formed at 220°C, just below the eutectic temperature, is estimated to be always larger than that of Ag_3Sn for the same wt.% of Cu or Ag, as shown graphically in Fig. 13. The second reason is that the bulk hardness of Cu_6Sn_5 (~4.5 GPa) is much higher than that of Ag_3Sn (~1.5 GPa).[21] Therefore, for the same amount of Ag or Cu, Sn-Cu solders are expected to be harder than Sn-Ag, assuming each IMC system has similar size and distribution characteristics.

CONCLUSIONS

The microstructure and mechanical properties of Pb-free Sn-rich solders were found to be strongly affected by alloying elements and cooling rate. The microstructure of Sn-rich solders consists of Sn dendrite cells, twin boundaries, and IMC particles, mostly precipitated along the cell boundaries. The EBSD study reveals fine cyclic twinning structures in Sn-Ag and the presence of general grain boundaries in Sn-Cu solders. The higher propensity to form cyclic twins in Sn-Ag over that in pure Sn and Sn-Cu could be explained by the higher solubility of Ag in Sn. The beach-ball-shaped twinning structure observed in Sn-Ag-Cu solder balls could be explained by the combined effects of Ag addition, promoting the fine cyclic twinning structure, and of the Cu addition, favoring the large grains. The addition of Cu to Sn is more effective than Ag addition in hardening of Sn-rich solders for the same wt.%, largely owing to their respective IMCs (Cu_6Sn_5 versus Ag_3Sn). The microhardness of Sn-rich solders with low Ag or Cu alloying elements is found to be better correlated with the characteristics of IMC particles (type, size, and distribution) than with the grain or twin structure. Twin boundaries exhibit no significant hardening effect.

ACKNOWLEDGEMENT

This work was supported by the Center for Electronic Packaging Materials (ERC) of the MEST/KOSEF (Grant No. R11-2000-085-08006-0).

REFERENCES

1. S.K. Kang and A.K. Sarkhel, *J. Electron. Mater.* 23, 701 (1994). doi:10.1007/BF02651362.
2. S.W. Jeong, J.H. Kim, and H.M. Lee, *J. Electron. Mater.* 33, 1530 (2004). doi:10.1007/s11664-004-0095-9.

3. S.K. Kang, W.K. Choi, D.-Y. Shih, D.W. Henderson, T. Gosselin, A. Sarkhel, C. Goldsmith, and K.J. Puttlitz, *Proc. 53rd Electronic Components and Technology Conf.* (Piscataway, NJ: IEEE, 2003), pp. 64–70.
4. S.K. Kang, W.K. Choi, D.-Y. Shih, D.W. Henderson, T. Gosselin, A. Sarkhel, C. Goldsmith, and K.J. Puttlitz, *JOM* 55, 61 (2003). doi:10.1007/s11837-003-0143-6.
5. E. Laine, E. Perfecto, B. Campbell, J. Wood, J. Busby, J. Garant, and L. Guerin, *Proc. 57th Electronic Components and Technology Conf.* (Piscataway, NJ: IEEE, 2007), pp. 1320–1325.
6. S. Ishikawa, T. Uchiyama, E. Hashino, T. Kohno, M. Tanaka, and K. Tatsumi, *Proc. 57th Electronic Components and Technology Conf.* (Piscataway, NJ: IEEE, 2007), pp. 872–877.
7. D. Kim, D. Suh, T. Millard, H. Kim, C. Kumar, M. Zhu, and Y. Xu, *Proc. 57th Electronic Components and Technology Conf.* (Piscataway, NJ: IEEE, 2007), pp. 1614–1619.
8. M. Uchida, H. Ito, K. Yabui, H. Nishiuchi, T. Togasaki, K. Higuchi, and H. Ezawa, *Proc. 57th Electronic Components and Technology Conf.* (Piscataway, NJ: IEEE, 2007), pp. 885–891.
9. T.R. Bieler, H. Jiang, L.P. Lehman, T. Kirkpatrick, and E.J. Cotts, *Proc. 56th Electronic Components and Technology Conf.* (Piscataway, NJ: IEEE, 2006), pp. 1462–1467.
10. D.W. Henderson, J.J. Woods, T.A. Gosselin, J. Bartelo, D.E. King, T.M. Korhonen, M.A. Korhonen, L.P. Lehman, E.J. Cotts, S.K. Kang, P. Lauro, D.-Y. Shih, C. Goldsmith, and K.J. Puttlitz, *J. Mater. Res.* 19, 1608 (2004). doi:10.1557/JMR.2004.0222.
11. L.P. Lehman, S.N. Athavale, T.Z. Fullem, A.C. Giamis, R.K. Kinyanjui, M. Lowenstein, K. Mather, R. Patel, D. Rae, J. Wang, Y. Xing, L. Zavalij, P. Borgesen, and E.J. Cotts, *J. Electron. Mater.* 33, 1429 (2004). doi:10.1007/s11664-004-0083-0.
12. A. Lalonde, D. Emelander, J. Jeannette, C. Larson, W. Rietz, D. Swenson, and D.W. Henderson, *J. Electron. Mater.* 33, 1545 (2004). doi:10.1007/s11664-004-0096-8.
13. B. Sundman, B. Jansson, and J.O. Andersson, *Calphad* 9, 153 (1985). doi:10.1016/0364-5916(85)90021-5.
14. U.R. Kattner and W.J. Boettinger, *J. Electron. Mater.* 23, 603 (1994). doi:10.1007/BF02653345.
15. J.-H. Shim, C.-S. Oh, B.-J. Lee, and D.N. Lee, *Z. Metallk.* 87, 205 (1996).
16. G. Ghosh, *Metab. Mater. Trans. A* 30A, 1481 (1999). doi:10.1007/s11661-999-0085-x.
17. A.U. Telang, T.R. Bieler, J.P. Lucas, K.N. Subramanian, L.P. Lehman, Y. Xing, and E.J. Cotts, *J. Electron. Mater.* 33, 1412 (2004). doi:10.1007/s11664-004-0081-2.
18. S.K. Kang, M.G. Cho, P. Lauro, D.-Y. Shih, *Proc. 57th Electronic Components and Technology Conf.* (Piscataway, NJ: IEEE, 2007), pp. 1597–1603.
19. M.G. Cho, S.K. Kang, and H.M. Lee, *J. Mater. Res.* 23, 1147 (2008). doi:10.1557/jmr.2008.0133.
20. S.K. Kang, M.G. Cho, D.-Y. Shih, S.-K. Seo, and H.M. Lee, *Proc. 58th Electronic Components and Technology Conf.* (Piscataway, NJ: IEEE, 2008), pp. 478–484.
21. H.-J. Albrecht, A. Juritza, K. Muller, W.H. Muller, J. Sterthaus, J. Villain, and A. Vogliano, *Proc. 5th Electronics Packaging Technology Conf.* (Piscataway, NJ: IEEE, 2003), pp. 726–731.